Applied Computer Science, vol. 20, no. 4, pp. 192–210
doi: https://doi.org/10.35784/acs-2024-47

Submitted: 2024-09-13 | Revised: 2024-11-11 | Accepted: 2024-11-20

Keywords: unsharp mask, guided filter, image sharpening, MRI images

Manar AL-ABAJI [0000-0001-9251-8920]*, *Zohair Al-AMEEN* [0000-0003-3630-2134]**

SHARPNESS IMPROVEMENT OF MAGNETIC RESONANCE IMAGES USING A GUIDED-SUBSUMED UNSHARP MASK FILTER

Abstract

Magnetic resonance imaging (MRI) is a key method for imaging human tissues and organs. The accuracy of medical diagnosis is greatly affected by the quality of MRI images. Sometimes, MRI images are obtained blurry due to various inevitable constraints related to the imaging equipment, which affects the detection of important features in the image. Several sharpening methods were introduced, but not all were successful in this task, as artifacts may be introduced, contrast may be changed, and high complexity may be involved. Thus, this paper introduces a guided-subsumed unsharp mask filter (GSUM) to improve the sharpness of MRI images. The GSUM utilizes an improved guided filter instead of the low-pass Gaussian filter and a dynamic sharpening parameter. The improved guided filter employs a hybrid procedure instead of the mean filter in the smoothing process and relies on an adaptive regularization parameter. The applied modifications eliminated the overshooting and halo effects of the original unsharp masking and the guided filter, resulting in better-quality images. The GSUM was tested with real-blurry MRI images, evaluated using three no-reference metrics, and compared with six other algorithms. The metric scores indicate that the proposed filter can surpass existing methods, as it produced better results with average readings of 24.2074 in PIQE, 0.6878 in BLUR, and 5.7944 in FISH. It also scored a fast computation time, averaging 0.3384 seconds.

1. INTRODUCTION

Medical imaging techniques are procedures for taking pictures of the human body or specific areas for scientific, medicinal, or diagnostic reasons. MRI is the most employed medical imaging method. MRIs are used to diagnose a wide range of diseases, especially those that affect the brain and nervous system, due to their superior accuracy in visualizing soft tissues (Singh & Choubey, 2021; Jeevakala & Therese, 2018). Blurriness in medical images can be caused by imaging equipment, the patient's movements, or the transmission method. Blurring makes the image's edges less intense, obscuring the visibility of the

* University of Mosul, College of Education for Pure Science, Department of Computer Science, Nineveh, Iraq, manar_alabaji@uomosul.edu.iq
** University of Mosul, University of Mosul Presidency, Computer Center, ICT Research Unit, Nineveh, Iraq, qizohair@uomosul.edu.iq

image's information and tiny details and affecting its clarity, which is crucial to the diagnosis and treatment process in the medical field (Habee, 2021).

Sharpness is strongly correlated with blur, significantly affecting how well an image is perceived (Li et al., 2016). It is a simple measurement of edge lucidity in a specific area of an image (Gui & Liu, 2011). Enhancing blurry features or bringing attention to fine details is the primary goal of image sharpening techniques. Sharpening also focuses on enhancing features in the high-frequency range by using the scaled edge information close to object boundaries (Zafeiridis et al., 2016; Chen, 2019). Sharpening is an essential pre-processing procedure that increases the contrast between the bright and dark areas to highlight edge details. It draws attention to the already present minor components, making the edges steeper. Most studies concentrate on improving the borders of subtle tissues or organs since they have a greater perceptual significance (Jeevakala & Therese, 2018).

During the past few years, there has been a growing amount of study on image sharpening with varying degrees of complexity depending on the concept, proposing several well-known methods in this field. Among the most well-known techniques are shock filtering (Osher & Rudin, 1990), unsharp masking (Ngo et al., 2020), Laplacian filtering (Yang, 2014), and neighborhood operators (Gui & Liu, 2011). Despite broad developments in computer vision and digital image processing, image sharpening is an active research subject because of various practical challenges like staircase (Calder et al., 2010), overshoot (Kheradmand & Milanfar, 2015), image noise amplifying (Sheppard et al., 2004), and over-sharpening (Kal et al., 2011) effects. These effects make using such sharpening methods in the medical field undesirable. As mentioned earlier, many concepts are applied for image sharpening. Among them, the unsharp mask has gained the attention of many researchers over the past years because it is fast and simple to apply. Still, it produces an overshoot effect, inevitably reducing the quality of the processed image. This effect makes the edges of the image appear to have noticeable white shades on either side (Cao et al., 2011). Thus, it is necessary to enhance the unsharp mask's processing capability to provide sharper and artifacts-free results. Even with the widespread prosperity of image sharpening, there is still a potential to improve this filter.

Hence, a guided-subsumed unsharp mask filter (GSUM) is presented in this study to enhance the acutance without causing any undesirable effects. In the proposed unsharp mask filter, the image is smoothed using an improved guided filter instead of the low-pass Gaussian filter, and the final resulting image is produced based on a dynamic sharpening parameter. As for the improved guided filter, the mean filter in the smoothing process was replaced by a hybrid filter, which uses the new weighted mean filter, and a modified Butterworth low-pass filter, which utilizes an adaptive regularization parameter. This method eliminates the undesirable overshoot and halo effects of the unsharp mask filter and produces sharp images with good perceptual quality. Lastly, the proposed filter was evaluated using three no-reference metrics and processing time. Then, its performance was compared with six other algorithms. The reading results from the metrics proved the performance abilities of the GSUM over the other algorithms, resulting in promising outcomes. The organization of this paper is as follows: Section 2 introduces a review of previous relevant research studies. Section 3 includes a detailed explanation of the original and improved methods. Section 4 presents a description and analysis of the performance comparison between the proposed filter and other algorithms. Lastly, the conclusion of the paper is contained in Section 5.

2. RELATED WORKS

This section explains a few research studies highlighting the fundamental concepts that have been applied previously in the image-sharpening field. In Jeevakala & Therese (2018), an innovative sharpness improvement technique that relies on the Laplacian pyramid (LP) and single-value decomposition (SVD) was presented. The suggested technique divides images into distinct and coarse sub-bands using multi-scale decomposition. Then, LP effectively captures edges, and the SVD approach improves the features of these edges. Better edge retention and detail refining are made possible by this method, which enhances the delicate tissue edges and raises the visual quality of magnetic resonance imaging. However, the lines and contours of low-contrast images introduce undesirable artifacts at the boundaries of subtle tissues. In Joseph et al. (2019), a fully adaptable unsharp mask was proposed for sharpening magnetic resonance images. The adapted filter objectively and adaptively calculates its operational parameters, including threshold and amount. By using this method, artifacts like overshoot and noise amplification can be avoided. This method produces sharp images by increasing the contrast in the areas adjacent to the edges, which leads to the appearance of "halos" around the edges.

In (Luo et al., 2020), A novel method based on information entropy was proposed. It relies on two primary techniques: information entropy and sharpening processing. The algorithm determines an adaptive threshold and computes the information entropy for segmented image blocks. Image blocks with entropy values below this threshold are sharpened. Although this method provides balanced sharpening, it requires more improvements, as artifacts appear on the filtered image. In Al-Ameen et al. (2020), an anisotropic diffusion-based unsharp mask filter is presented. It uses an altered anisotropic diffusion filter instead of the conventional low-pass Gaussian filter. This filter improves the sharpness of digital images by lessening the overshoot effect that unsharp masking techniques suffer from and produces images of higher quality with adequate details, a natural look, and illumination that nearly mimics the source images. However, it tended to suppress some highlights of the outer region. In Deng et al. (2021), a new filter formulation based on Laplacian combined the sharpening and smoothing operations simultaneously. A patch interpolation model, a critical component in the filter, was employed to improve the filter's edge awareness and enable it to maintain significant image features during processing better. Also, depending on the generalized gamma distribution to estimate the parameter, this statistical method helps improve the filter's functionality and ability to adjust to different image characteristics. However, this method produced an overshoot effect in the processed image.

In Huang (2021), an improving image sharpness approach based on the green function is proposed. It uses the retinex model, renowned for its capacity to amplify visual details. Additionally, the solution of Poisson's equation in the gradient domain is a crucial component of the suggested approach because it ensures that crucial gradient information is kept intact throughout the enhancement process. Although this algorithm can enhance an image's sharpness and contrast, it requires many computations. In Edla et al. (2022), a maximum local variation-based unsharp masking was proposed to address the problem of low sharpness in MRI images. This algorithm depends on a locally adaptive 2D Gaussian filter, and it aims to enhance the MR images' sharpness, which is essential for accurate diagnosis and treatment. Although this algorithm produces acceptable sharpeners and

preserves the mean brightness level of the images without any overshoot or intensity saturation, it depends on user-defined parameters, and this may result in producing images with unnatural appearances and noise amplifying if the parameters are not carefully adjusted. Also, the dependency on locally adaptive filters results in longer processing times, mainly when applied to high-resolution images. Table 1 offers a summary of the reviewed studies.

Tab. 1. The summary of the reviewed research studies

Year	Concept	Advantages	Disadvantages
2018	Laplacian pyramid single-value decomposition	Enhances the delicate tissue edges	Introduces undesirable artifacts at the boundaries
2019	Unsharp mask	Avoids overshoot and noise amplification	Produces haloes around the edges
2020	Information entropy	Provides balanced sharpening	Requires more improvements
2020	Anisotropic diffusion unsharp mask	Produces adequate details	Suppresses some highlights of the outer region
2021	Laplacian filter	Maintains the key features	Introduces the overshoot effect
2021	Green function and retinex model	Enhances the sharpness and contrast	Requires many computations
2022	Maximum local variation unsharp masking	Preserves the brightness without any overshoot or intensity saturation	Depends on user-defined parameters
2023	Weighted spatial derivative	Prevents noise amplification Fewer operational parameters	Difficulties in parameter selection may lead to unnatural appearances
2024	Wavelet fusion with unsharp mask	Avoids generating artifacts	Involves sophisticated processing

In Simi et al. (2023), a nonlinear amplification of spatial derivative (NASD) was introduced. The NASD uses an inverse method to estimate the enhanced image from the amplified spatial derivative. The amplification factor at each pixel position is determined using a nonlinear function of the average of the absolute values of the gradients over eight different orientations at that place to prevent the amplification of noise. The NASD produces a better sharpness-to-noise ratio. Although the NASD algorithm uses fewer operational parameters than conventional techniques, some factors must be carefully adjusted, including noise suppression and acuity control parameters. Otherwise, it may lead to unnatural appearances in the results. In Bogdan et al. (2024), a multiscale method was proposed that integrates the wavelet image fusion with multiple dilated unsharp mask algorithms. In this method, the image is analyzed at multiple scales using a dilated unsharp mask to get details from different scales and orientations to sharpen both the subtle and the prominent image details. After that, a wavelet fusion combines these details adaptively into a single, sharp image. Despite this method showing improved image sharpness and avoiding noticeable artifacts, it involves sophisticated processing. The reviewed studies have shown that various concepts have been used for image sharpening; they share the goal of rapidly providing sharp results while avoiding artifact generation. However, not all these methods succeeded in

achieving this goal, as some of them required excessive calculations and long processing time, and some produced unnatural sharpness, artifacts, or insufficient enhancement. Therefore, developing a method that provides satisfactory results is necessary, and the opportunity to achieve this task is still available.

3. PROPOSED FILTER

This section provides a comprehensive description of the proposed sharpening filter. The suggested filter begins by acquiring the blurred image. Next, the improved guided filter is implemented to smooth the image and attenuate its high-frequency components. The smoothing process relies on the new weighted mean filter and a modified Butterworth low-pass filter. It also utilizes an adaptive regularization parameter (this parameter determines what edge should be preserved) to avoid generating halo artifacts. Afterward, the outcome of this procedure is utilized as an input for the unsharp mask filter, which uses a dynamic sharpening parameter to produce the final image. The following sub-sections provide full explanations of the main stages of the proposed filter to provide a thorough understanding of its operational details.

3.1. Guided filter

Before explaining the improved guided filter, we will briefly overview the classical guided filter introduced by He et al. (2013). It utilizes a local linear model to produce the filtering output. It considers the content of a guiding image, which can be the same input or another distinct image. The local linear model guarantees that the output-filtered image will have an edge only if the guided image has an edge. The guided filter is not only a rapid edge-preserving smoothing filter but also effectively prevents the occurrence of "gradient reversal" artifacts (He et al., 2013; Zhang & Wu, 2023). The basic idea of guided filtering is to establish a linear relationship between the output image Q and the guided image I. This relationship defined inside a window w_k, centered at the pixel k, can be mathematically expressed as:

$$Q_i = a_k I_i + b_k \,, \quad \forall i \in w_k \tag{1}$$

where (a_k, b_k) are linear coefficients supposed to be constant in w_k. To find these linear coefficients, a cost function E is used inside the window w_k to minimize the difference between the input P_i and the output Q_i while preserving the linear model. The function E is expressed as follows:

$$E(a_k, b_k) = \sum_{i \in w_k} \left((a_k I_i + b_k - P_i)^2 + \epsilon a_k^2 \right) \tag{2}$$

where $\in$ is a regularization parameter that prevents the a_k value from increasing excessively, the values of a_k and b_k that yield the best results are calculated as:

$$a_k = \frac{\frac{1}{|w|}\sum_{i \in w_k} I_i P_i - \bar{I}_k \bar{P}_k}{\sigma_k^2 + \epsilon} \tag{3}$$

$$b_k = \bar{P}_k - a_k \bar{I}_k \tag{4}$$

where $\bar{I}_k$ and σ_k^2 represent the mean and variance of I in the w_k , $\bar{P}_k$ is the mean of P in the w_k, and $|w|$ represent the number of pixels within w_k . Finally, the filter output is computed as:

$$Q_i = \bar{a}_i I_i + \bar{b}_i \tag{5}$$

where $\bar{a}_i = \frac{1}{|w|}\sum_{k \in w_i} a_k$ and $\bar{b}_i = \frac{1}{|w|}\sum_{k \in w_i} b_k$, which are the outputs of an average filter. However, the guided filter has some drawbacks. One of them is that the guided filters focus the blurring effect mostly on the edges, resulting in the appearance of halos artifacts, which diminishes the image's visual fidelity. Halo artifacts primarily occur because of the fixed regularization parameter in the guided filter, which governs the filtering process (Shi et al., 2021). Another problem arises when applying the guided filter to transfer the structure from the guidance to the filtering output. Even if the filtering input is smooth, it is still possible for noise to be copied to the filtering output if the guidance contains noise. Resulting in unforeseen noise in the filtered output, referred to as guidance noise artifact (Zhang & Wu, 2023).

3.2. Butterworth low-pass filter

The Butterworth low-pass filter is a popular technique used for image blurring. The system keeps frequencies inside the radius D_0 and discards values outside to achieve a progressive change from 0 to 1. The equation for a Butterworth low-pass filter of order n and a cutoff frequency D_0 is given as follows (Sadah et al., 2013):

$$H(u,v) = \frac{1}{1+\left(\frac{D(u,v)}{D_0}\right)^{2n}} \tag{6}$$

where $D(u,v)$ is the distance between the point (u,v) and the frequency center, and $H(u,v)$ is the blurring mask produced by the Butterworth low-pass filter. To filter a given image, the first step is to transform the input image to the frequency domain, represented by $A(u,v)$. Next, the image is multiplied by $H(u,v)$ using the following equation:

$$B(x,y) = ifft[A(u,v).H(u,v)] \tag{7}$$

where $B(x,y)$ represents the final filtered image. In this paper, an adjusted version of the above filter is utilized, where the order n parameter is eliminated to decrease the number of inputs to the hybrid filter and achieve good blurring outcomes. The following equations illustrate the adjustment (Al-Ameen et al., 2019):

$$\widehat{H}(u,v) = \frac{1}{1+\left(\frac{\tilde{D}(u,v)}{D_0}\right)^2} \tag{8}$$

$$F2(x,y) = ifft\left[I(u,v).\widehat{H}(u,v)\right] \tag{9}$$

where $\widehat{D}(u,v)$ is computed from the guided image *I(x,y)* after transform it to the frequency domain, $\widehat{H}(u,v)$ is the blurring mask for the guided image; *F2(x,y)* is the final blurred result.

3.3. Weighted mean filter

The weighted mean filter is a smoothing filter. It has better effects on minimizing blurring throughout the smoothing phase and edge preservation capabilities than a simple mean filter due to its ability to diminish the influence of distant pixels, which are less likely to represent the actual pixel value accurately. This is done by assigning varying weights to pixels based on their distance to the central pixel. Following are examples of 3 × 3 smoothing (weighted mean) filters (Li et al., 2021):

$$w1 = \begin{bmatrix} 1 & 1 & 1 \\ 1 & 2 & 1 \\ 1 & 1 & 1 \end{bmatrix} \qquad w2 = \begin{bmatrix} 1 & 2 & 1 \\ 2 & 4 & 2 \\ 1 & 2 & 1 \end{bmatrix}$$

This study utilized a modified weighted mean filter for smoothing after conducting experiments on the weighted mean filter. It yielded superior outcomes in the smoothing process. A modified weighted mean filter is as follows:

$$w = \begin{bmatrix} 0.7 & 1 & 0.7 \\ 1 & 2 & 1 \\ 0.7 & 1 & 0.7 \end{bmatrix}$$

The smoothed image *F1* is computed as follows (Gonzalez & Woods, 2008):

$$F1(x,y) = \frac{\sum_{i=-k}^{k}\sum_{j=-k}^{k} w(i,j)I(x+i,y+j)}{\sum_{i=-k}^{k}\sum_{j=-k}^{k} w(i,j)} \tag{10}$$

where *k* is the neighborhood radius, *I* is the guided image, *I*(x+i, y+j) represents the pixel intensity at the neighborhood position, *w(i,j)* represents the weight assigned to the pixel at point *i*,*j*.

3.4. Adjusted guided filter

As mentioned above, the classical guided filter has some drawbacks that must be addressed. This paper proposes methods to attenuate these drawbacks and obtain a smoothed free-artifact image. Firstly, a spatially varying adaptive regularization parameter is employed instead of a fixed one to eliminate the halo artifacts, using edge-aware weighting obtained from the Sobel gradient magnitude(*S_GM*) for the guided image. This offers insight into the strength and orientation of edges. *S_GM* is calculated as follows (Holder & Tapamo, 2017):

$$S\_GM = \sqrt{G_x^2 + G_y^2} \tag{11}$$

where G_x and G_y are the horizontal and vertical approximations of the derivatives, respectively, obtained by convolving the guided image *I(x,y)* with horizontal and vertical

Sobel operator masks. Now, we can replace the fixed ϵ by the adaptive regularization parameter $\frac{\epsilon}{S\_GM}$.

Secondly, to address the problem of guidance noise artifacts, we proposed a hybrid filter instead of the box filtering (mean filter) used in the classical guided filter. The hybrid filter integrates a new weighted mean filter with a modified Butterworth low-pass filter in the smoothing process. The hybrid filter (*WM_B*) is constructed using the following formula:

$$WM\_B = \alpha \times F1 + (1 - \alpha) \times F2 \tag{12}$$

where α is a constant; its suitable value is 0.65. *F1* represents the result of the weighted mean filter, and *F2* represents the result of the modified Butterworth filter. The final improved guided filter formulas are now modified as the proposed weighting *S_GM* in Equation (11) is incorporated into the cost function *E* in Equation (2). The new cost function formula is defined as:

$$E(a_k, b_k) = \sum_{i \in w_k} \left((a_k I_i + b_k - P_i)^2 + \frac{\epsilon}{S\_GM} a_k^2 \right) \tag{13}$$

The values of a_k and b_k that yield the best results based on the new cost function formula are calculated as:

$$\alpha_k = \frac{\overline{\overline{I_i P_i}} - \overline{\overline{I_k}}.\overline{\overline{P_k}}}{\sigma_k^2 + \frac{\epsilon}{S\_GM}} \tag{14}$$

$$b_k = \overline{\overline{P_k}} - \alpha_k \overline{\overline{I_k}} \tag{15}$$

where $\overline{\overline{I}}$, $\overline{\overline{P}}$ represent *I*, *P* after processing by the hybrid filter (*WM_B*), $\overline{\overline{IP}}$ represent $I \times P$ after processing by the hybrid filter (*WM_B*). The final output of the improved guided filter is computed as follows:

$$Q_i = \alpha_i I_i + b_i \tag{16}$$

3.5. Proposed unsharp masking

This filter is used in several imaging applications to enhance the acutance. The process entails subtracting a blurred version of an image from the original image and then adding the outcome back to the original image. The unsharp mask filter is defined as follows (Kim & Allebach, 2005):

$$U(x, y) = P(x, y) + \lambda[P(x, y) - G(x, y)] \tag{17}$$

where *(x,y)* are the coordinates, *P* is the original image, *G* is the image *P* after filtered by low pass Gaussian filter, *U* is the sharp image, and λ is the sharpening parameter. In this study, a dynamic sharpening parameter λ is used instead of a fixed one to control the degree of amplification in the high-frequency range and adaptively enhance image details. This method utilizes image variance and calculates the difference between each pixel and its neighboring pixels to modify the sharpening parameter dynamically. As a result, pixels at

various locations are enhanced adaptively. The calculation of the unsharp mask filter becomes as follows:

$$N\_d = P(i-1,j) - P(i,j) \tag{18}$$

$$S\_d = P(i+1,j) - P(i,j) \tag{19}$$

$$E\_d = P(i,j+1) - P(i,j) \tag{20}$$

$$W\_d = P(i,j-1) - P(i,j) \tag{21}$$

$$T\_diff(x,y) = |N\_d + S\_d + E\_d + W\_d| \tag{22}$$

$$\lambda(x,y) = \frac{exp(-\sigma^2)}{0.18+T\_diff} \tag{23}$$

$$U(x,y) = P(x,y) + \lambda(x,y)[P(x,y) - Q(x,y)] \tag{24}$$

where *(x,y)* are the coordinates, σ^2 is the variance of *P*, *Q* is the output of the improved guided filter, *T_diff* is the absolute total difference between each pixel and its neighboring pixels, and *N_d, S_d, E_d,* and *W_d* represent the detected differences at the north, south, east, and west, respectively. The GSUM filter is further described in the following pseudocode.

The pseudocode of the proposed GSUM filter
Input: Low-acutance image $P_{(x,y)}$, ∈ Set guided image $I = P$ Compute the smoothed image F1 using Eq.10 Compute the smoothed image F2 using Eq.9 Compute the improved guided filter using Eq.16 Compute the sharp image using Eq.24 Output: Sharpen image $U_{(x,y)}$

4. RESULTS AND DISCUSSION

This section presents the results of the relevant comparisons and analyses to verify the efficiency of the proposed GSUM filter. The evaluation is based on about 150 real blurry images taken from the CTisus website, the Johns Hopkins Hospital repository for real medical images, which can be reached at https://www.ctisus.com/. The GSUM's ability to sharpen dissimilar images is also evaluated by comparing it with several existing algorithms, such as generalized unsharp masking (GUM) (Deng, 2010), nonlinear unsharp masking (NUM) (Ngo et al., 2020), low-light image enhancement based on a sharpening-smoothing image filter (LL_SSIF) (Demir & Kaplan, 2023), edge-aware smoothing-sharpening filter (EA_SSIF) (Deng et al., 2021), anisotropic diffusion-based unsharp masking (ADUSM) (Al-Ameen et al., 2020), and amended unsharp masking (AUSM) (Al-Ameen et al., 2019). As for the image quality evaluation methods, three no-reference methods are utilized, namely, no-reference perception-based image quality evaluator (PIQE) (Venkatanath et al., 2015),

no-reference perceptual blur metric (Blur metric) (Crete et al., 2007), and fast image sharpness metric (FISH) (Vu & Chandler, 2012).

The PIQE metric utilizes local information to forecast an image's quality and quantifies distortion visibility. A lower index means reduced distortion visibility and higher visibility. The Blur metric is sufficient to estimate the blur artifact in an image. It is based on discriminating between different levels of blur perceptible on the same picture. Its value ranges from 0 to 1, respectively, the best and the worst quality regarding blur perception. The FISH measures the perceived sharpness of the image. It utilizes a three-level separable DWT to decompose the input image. Then, the estimating process is done based on a weighted geometric mean for the energies belonging to DWT's sub-bands. The higher the FISH index, the stronger the perceived sharpness. Figures 1 and 2 present the experimental results of applying the GSUM filter. Tables 2 and 3 present the recorded metrics scores related to the image samples in Figures 1 and 2. Figures 3 to 6 show the results when compared with other sharpening algorithms. Tables 4 to 7 present the recorded metrics scores and the processing times. Figures 7 to 10 show the recorded metrics scores and the processing times as charts.

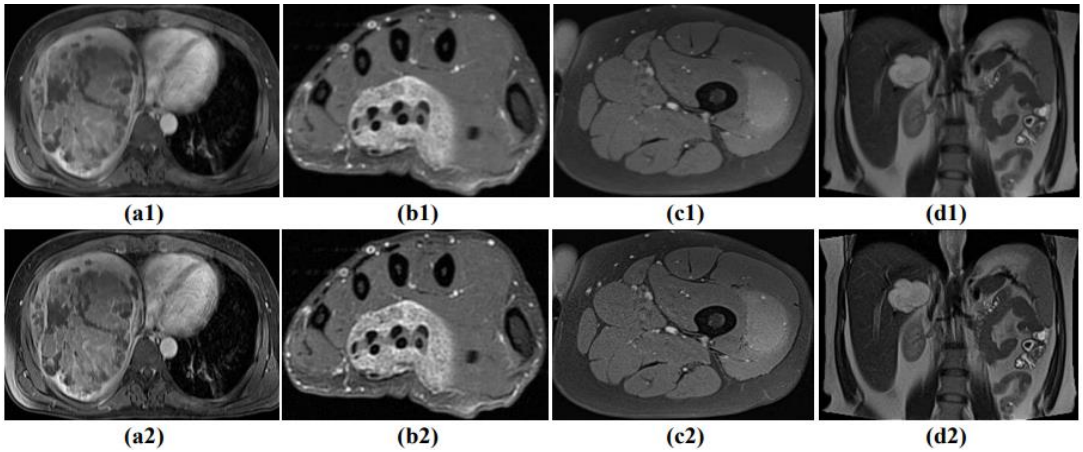

Fig. 1. Results of the GSUM with real-degraded MR images (Set 1). (a1-d1) are real-blurred MR images; (a2-d2) are images processed by the GSUM filter

Tab. 2. The values of PIQE, BLUR, and FISH metrics for sample images in Figure 1

Metrics		**Set 1**				**Average**
		a	**b**	**c**	**d**	
PIQE ↓	blur image	52.2279	47.3474	46.2581	52.4226	49.5640
	GSUM filter	33.1688	26.5412	37.7157	35.6862	33.2780
BLUR ↓	blur image	0.8007	0.8234	0.7161	0.8316	0.7930
	GSUM filter	0.7260	0.7049	0.6453	0.7449	0.7053
FISH ↑	blur image	2.3404	2.2321	2.2478	1.7349	2.1388
	GSUM filter	6.1208	6.1004	5.8429	5.1334	5.7994

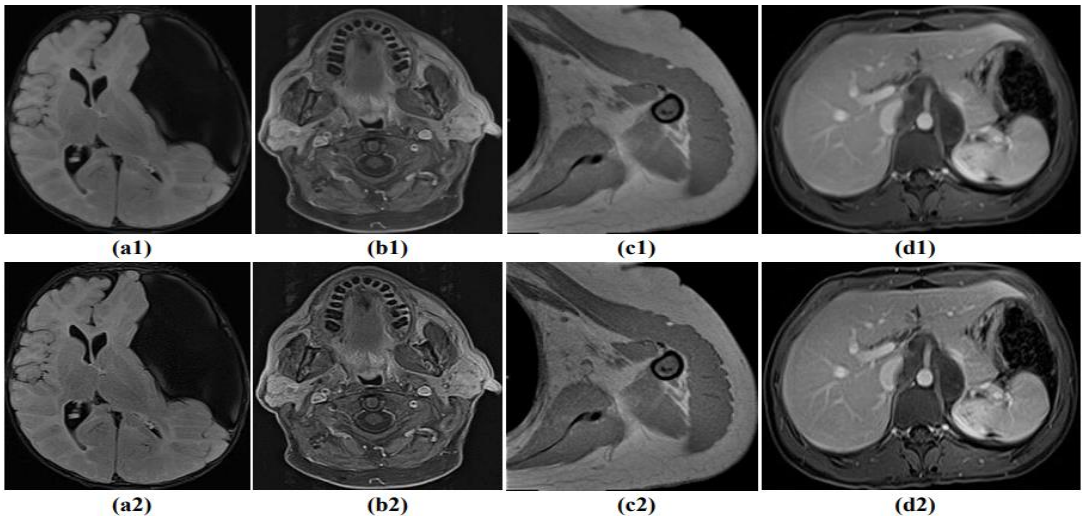

Fig. 2. Results of the GSUM with real-degraded MR images (Set 2). (a1-d1) are real-blurred MR images; (a2-d2) are images processed by the GSUM filter

Tab. 3. The values of PIQE, BLUR, and FISH metrics for sample images in Figure 2

Metrics		**Set 2**				**Average**
		a	**b**	**c**	**d**	
PIQE ↓	blur image	54.9516	49.7475	30.9298	59.2502	48.7198
	GSUM filter	37.8877	30.3014	25.9352	37.0035	32.7820
BLUR ↓	blur image	0.7504	0.7592	0.7288	0.7989	0.7593
	GSUM filter	0.6504	0.6597	0.6666	0.6915	0.6671
FISH ↑	blur image	2.1163	2.6171	1.9400	2.1604	2.2085
	GSUM filter	5.4920	6.5835	5.4120	5.7854	5.8182

Figures 1 and 2 show that the resulting images appear more natural with sufficient details and have good illumination like their degraded counterparts. Thus, the proposed method produces highly sharp images without causing any visual artifacts. This explains why it obtains better average values than its degraded counterpart in PIQE, BLUR, and FISH metrics, as shown in Tables 2 and 3.

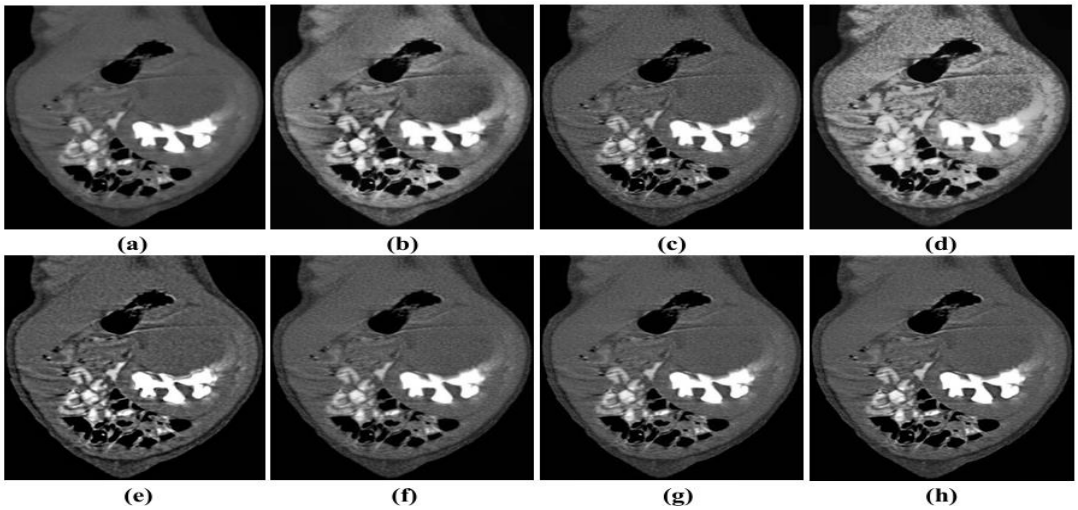

Fig. 3. The comparison outcome using real-blurred MR image (Set 1). (a) the original blurred MR image; images from (b-h) are obtained by (b) GUM, (c) NUM, (d) LL_SSIF, (e) EA_SSIF, (f) ADUSM, (g) AUSM, (h) Proposed GSUM filter

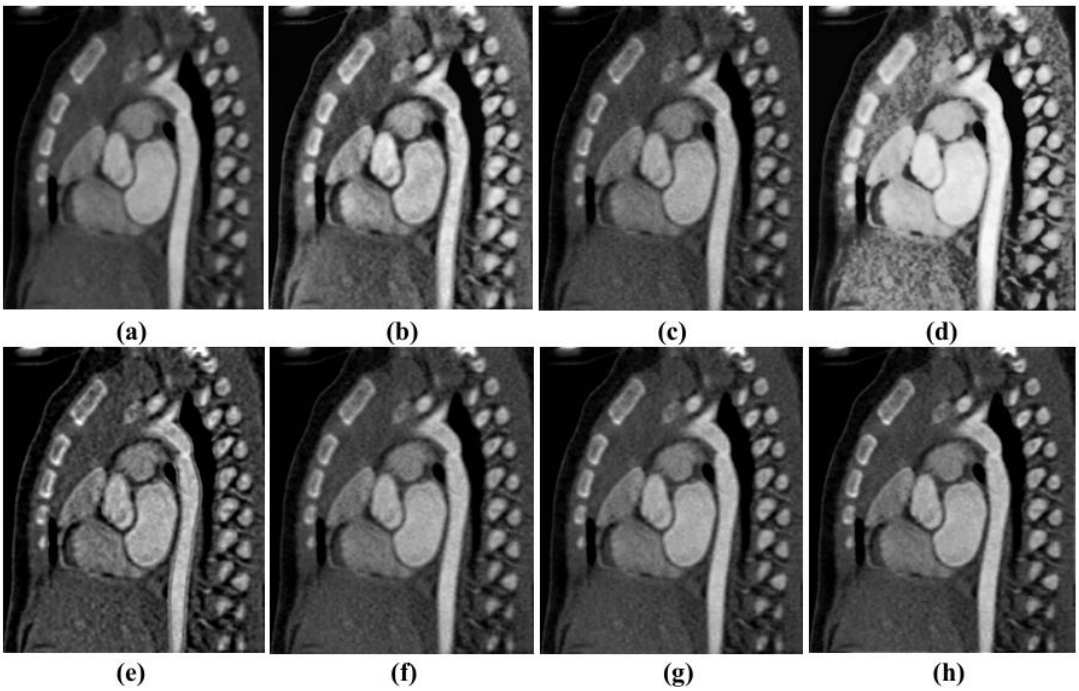

Fig. 4. The comparison outcome using real-blurred MR image (Set 2). (a) the original blurred MR image; images from (b-h) are obtained by (b) GUM, (c) NUM, (d) LL_SSIF, (e) EA_SSIF, (f) ADUSM, (g) AUSM, (h) Proposed GSUM filter

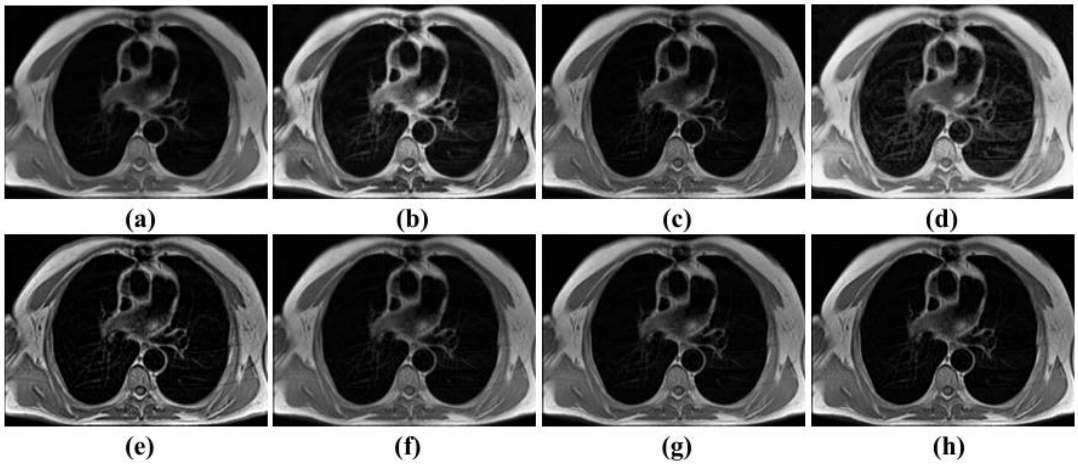

Fig. 5. The comparison outcome using real-blurred MR image (Set 3). (a) the original blurred MR image; images from (b-h) are obtained by (b) GUM, (c) NUM, (d) LL_SSIF, (e) EA_SSIF, (f) ADUSM, (g) AUSM, (h) Proposed GSUM filter

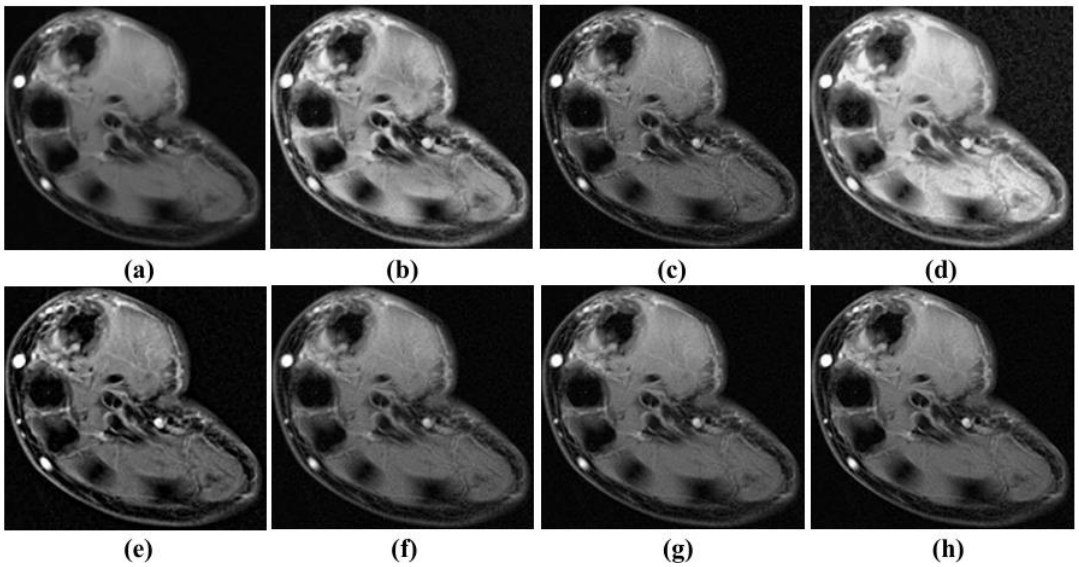

Fig. 6. The comparison outcome using real-blurred MR image (Set 4). (a) the original blurred MR image; images from (b-h) are obtained by (b) GUM, (c) NUM, (d) LL_SSIF, (e) EA_SSIF, (f) ADUSM, (g) AUSM, (h) Proposed GSUM filter

Tab. 4. The values of the PIQE ↓ metric

Fig.	GUM	NUM	LL_SSIF	EA_SSIF	ADUSM	AUSM	Proposed
3	33.6553	28.0730	37.5335	34.6899	21.8829	25.6985	14.6384
4	56.6545	54.5559	50.0052	53.7705	35.4017	41.3351	21.6108
5	62.6822	59.3607	68.4821	59.7502	42.7271	49.1641	39.1730
6	50.8885	46.4142	53.1515	49.2083	30.7943	37.3876	21.4075
Average	50.9701	47.1010	52.2931	49.3547	32.7015	38.3963	24.2074

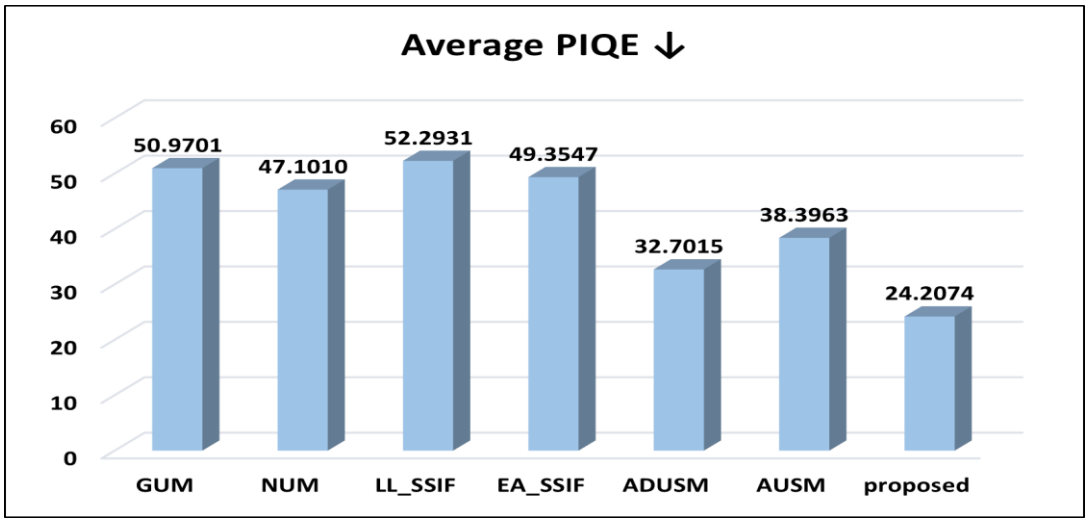

Fig. 7. The chart of average reading for PIQE measure

Tab. 5. The values of the Blur ↓ metric

Fig.	GUM	NUM	LL_SSIF	EA_SSIF	ADUSM	AUSM	Proposed
3	0.6811	0.6599	0.6930	0.7004	0.6758	0.6741	0.6434
4	0.7991	0.7325	0.8043	0.8149	0.7614	0.7695	0.7397
5	0.7548	0.7235	0.7833	0.7927	0.7424	0.7692	0.7220
6	0.7070	0.6626	0.7244	0.7342	0.6778	0.6853	0.6462
Average	0.7355	0.6946	0.7513	0.7606	0.7144	0.7245	0.6878

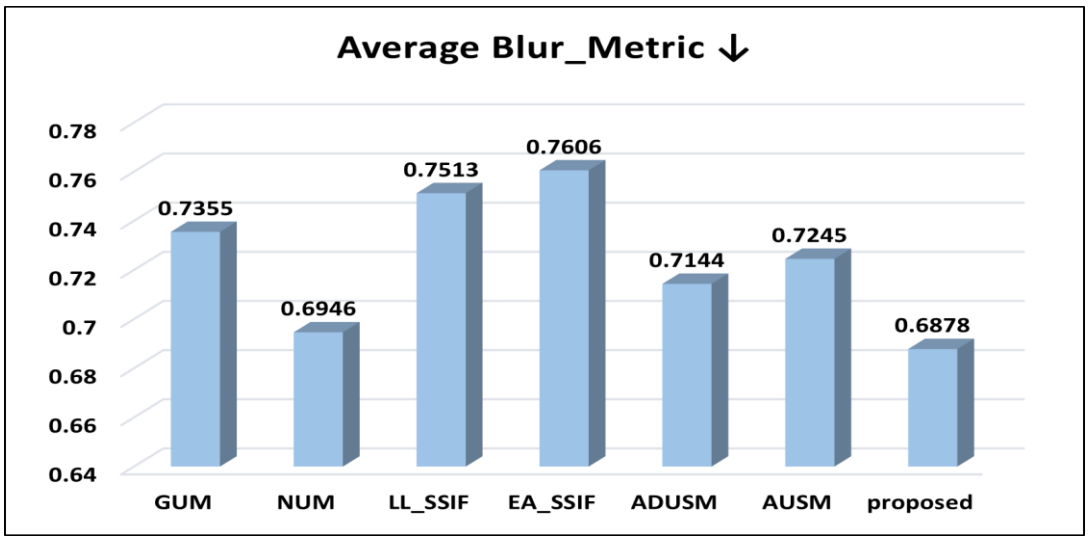

Fig. 8. The chart of average reading for Blur measure

Tab. 6. The values of the FISH ↑ metric

Fig.	GUM	NUM	LL_SSIF	EA_SSIF	ADUSM	AUSM	Proposed
3	6.2466	6.5558	6.5078	5.9690	5.5126	5.6657	7.3542
4	4.0132	3.9323	4.1992	3.4387	3.4655	3.2515	4.6084
5	4.4086	4.2995	3.7747	3.7153	3.6275	3.2611	4.9649
6	5.6240	5.5649	5.1274	4.8438	4.8769	4.6888	6.2502
Average	5.0731	5.0881	4.9023	4.4917	4.3706	4.2168	5.7944

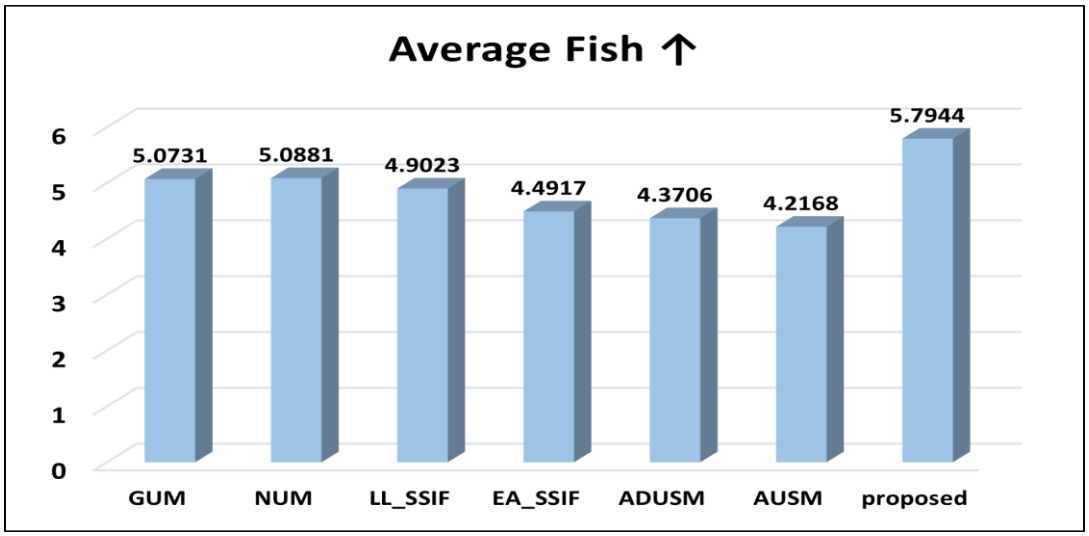

Fig. 9. The chart of average reading for FISH measure

Tab. 7. The values of the Runtimes ↓ (in seconds)

Fig.	GUM	NUM	LL_SSIF	EA_SSIF	ADUSM	AUSM	Proposed
3	0.2160	0.8461	0.2997	0.3110	0.4701	2.9728	0.3056
4	0.2109	0.8217	0.2993	0.2990	0.4770	3.0797	0.3727
5	0.2917	1.4638	0.4331	0.4441	0.7333	5.1217	0.4534
6	0.1786	0.7246	0.1877	0.2040	0.2825	2.1322	0.2220
Average	0.2243	0.9641	0.3049	0.3145	0.4907	3.3266	0.3384

The comparison results in Figures 3 to 10 and Tables 4 to 7 show that the proposed GSUM filter performed satisfactorily. It recorded the best in PIQE, Blur, and FISH measures, providing images with adequate sharpness without any obvious defects. It also has a fast computation time. Despite providing well-sharpened edges, the GUM attained third place in the FISH metric and had the fastest processing time since it noticeably changed both the contrast and the brightness of the results. This change reduced the visual quality, thus scoring sixth in PIQE and fifth in Blur metrics. Although the NUM recorded is slower in processing time, it provides good sharp edges, as recorded by the Blur and FISH metrics, where it gets the second-best values but scores moderately in PIQE.

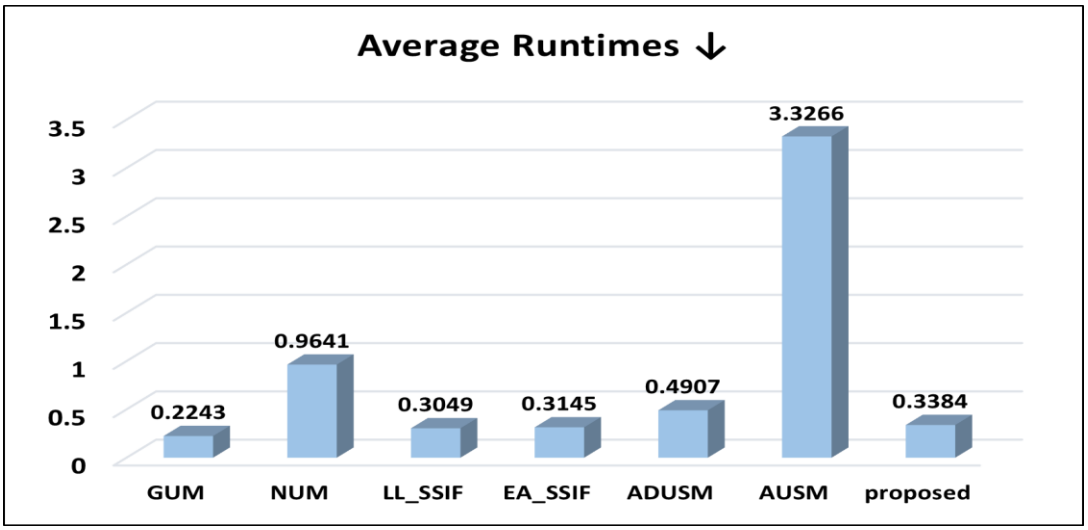

Fig. 10. The chart of average reading for Runtime

The LL_SSIF method was unsuccessful in delivering images with sufficient sharpness, which explains why it got a moderate FISH score and was ranked sixth in Blur. It also introduced an unwanted artifact and increased brightness in the resulting image, which reduced its integrity, as obvious from the worst PIQE score it attained. It was also ranked as having the second-fastest processing time. The EA_SSIF method introduced an overshooting effect. This effect makes the edges of the image appear to have noticeable white shades on either side, reducing the quality and information integrity. It also resulted in a slight increase in noise, scoring fifth in PIQE, seventh in Blur, and fifth in FISH. It was also the third fastest method.

In contrast, the results of ADUSM and AUSM have good visual quality, obtaining the second and third ranks in PIQE, respectively. However, there is still some blurring, which affects the sharpness of the edges. This explains why ADUSM gets the third and sixth scores in Blur and FISH metrics, respectively. It also has slow implementation, while AUSM gets the fourth and seventh scores in Blur and FISH metrics, respectively. It has the slowest processing time. To summarize, improving a standard filter to produce better results is difficult. This paper presents the GSUM filter, which gives acceptable results and satisfactory performances. The images produced by the GSUM filter have good sharpness, adequate brightness, natural contrast, and no artifacts, which makes this method suitable for many real-world applications, especially medical-related ones.

5. CONCLUSION

This study introduces a developed GSUM filter that enhances the acutance of MR images without causing undesirable effects. The improvements include using a modified guided filter with a new weighted mean filter and a modified Butterworth low pass filter instead of the mean filter in the smoothing process, relying on an adaptive regularization parameter. Subsequently, the outcome of this procedure is utilized as an input for the unsharp mask filter, resulting in the final image using a dynamic sharpening parameter. The GSUM filter

is tested with many real-blurry images from a credible website to evaluate its sharpening abilities. The comparison results are then assessed with four measures. Accordingly, the GSUM filter performed satisfyingly, generating sharp MR images with enhanced visual quality and providing a more natural appearance, adequate detail, and optimal lighting without introducing visual artifacts. In addition, the GSUM filter performances are evident from the results produced by the used measures. Moreover, the results of the GSUM filter were shown to a radiologist and MRI specialist, Dr. Naser Kashmola. He examined the resulting images and remarked that they were better than their degraded counterparts in sharpness and detail clarity. For future work, better automation methods can be exploited for improved computerization.

Author Contributions

The PhD student Manar A. Al-Abaji contributed to data gathering, analysis, and algorithm development. The supervisor, Zohair Al-Ameen, modified and advised on the technique used, the algorithm's development, the analysis of results, and the article review.

Acknowledgments

We want to thank Dr. Naser Kashmola, a radiology specialist, for evaluating and endorsing the results of the proposed GSUM filter.

REFERENCES

Al-Ameen, Z., Al-Healy, M. A., & Hazim, R. A. (2020). Anisotropic diffusion-based unsharp masking for sharpness improvement in digital images. *Journal of Soft Computing and Decision Support Systems*, *7*(1), 7-12.

Al-Ameen, Z., Muttar, A., & Al-Badrani, G. (2019). Improving the sharpness of digital image using an amended unsharp mask filter. *International Journal of Image, Graphics and Signal Processing*, *11*(3), 1-9. https://doi.org/10.5815/ijigsp.2019.03.01

Bogdan, V., Bonchiș, C., & Orhei, C. (2024). An image sharpening technique based on dilated filters and 2D-DWT image fusion. *9th International Joint Conference on Computer Vision, Imaging and Computer Graphics Theory and Applications (VISAPP)* (pp. 591-598). SciTePress. https://doi.org/10.5220/0012416600003660

Calder, J., Mansouri, A., & Yezzi, A. (2010). Image sharpening via Sobolev gradient flows. *SIAM Journal on Imaging Sciences*, *3*(4), 981-1014. https://doi.org/10.1137/090771260

Cao, G., Zhao, Y., Ni, R., & Kot, A. C. (2011). Unsharp masking sharpening detection via overshoot artifacts analysis. *IEEE Signal Processing Letters*, *18*(10), 603-606. https://doi.org/10.1109/LSP.2011.2164791

Chen, T. J. (2019). An adaptive image sharpening scheme. *Multi Conference on Computer Science and Information Systems, MCCSIS 2019 - Proceedings of the International Conferences on Interfaces and Human Computer Interaction 2019, Game and Entertainment Technologies 2019 and Computer Graphics, Visualization, Comp* (pp. 396-400). International Association for development of the information society. https://doi.org/10.33965/g2019_201906c056

Crete, F., Dolmiere, T., Ladret, P., & Nicolas, M. (2007). The blur effect: perception and estimation with a new no-reference perceptual blur metric. *Human Vision and Electronic Imaging*, *6492*. https://doi.org/10.1117/12.702790

Demir, Y., & Kaplan, N. H. (2023). Low-light image enhancement based on sharpening-smoothing image filter. *Digital Signal Processing*, *138*, 104054. https://doi.org/10.1016/j.dsp.2023.104054

Deng, G. (2010). A generalized unsharp masking algorithm. *IEEE Transactions on Image Processing*, *20*(5), 1249-1261. https://doi.org/10.1109/TIP.2010.2092441

Deng, G., Galetto, F., Alnasrawi, M., & Waheed, W. (2021). A guided edge-aware smoothing-sharpening filter based on patch interpolation model and generalized gamma distribution. *IEEE Open Journal of Signal*

Processing, *2*, 119-135. https://doi.org/10.1109/OJSP.2021.3063076
Edla, D. R., Simi, V. R., & Joseph, J. (2022). A noise-robust and overshoot-free alternative to unsharp masking for enhancing the acuity of MR images. *Journal of Digital Imaging*, *35*, 1041-1060. https://doi.org/10.1007/s10278-022-00585-z
Gonzalez, R. C., & Woods, R. E. (2008). *Digital Image Processing, 3rd Edition*. Pearson Prentice Hall.
Gui, Z., & Liu, Y. (2011). An image sharpening algorithm based on fuzzy logic. *Optik*, *122*(8), 697-702. https://doi.org/10.1016/j.ijleo.2010.05.010
Habee, N. J. (2021). Performance enhancement of medical image fusion based on DWT and sharpening Wiener filter. *Jordanian Journal of Computers and Information Technology*, *7*(2), 118-129. https://doi.org/10.5455/jjcit.71-1610049522
He, K., Sun, J., & Tang, X. (2013). Guided image filtering. *IEEE Transactions on Pattern Analysis and Machine Intelligence*, *35*(6), 1397-1409. https://doi.org/10.1109/TPAMI.2012.213
Holder, R. P., & Tapamo, J. R. (2017). Improved gradient local ternary patterns for facial expression recognition. *EURASIP Journal on Image and Video Processing*, *2017*, 42. https://doi.org/10.1186/s13640-017-0190-5
Huang, Q. (2021). An image sharpness enhancement algorithm based on green function. *Traitement Du Signal*, *38*(2), 513-519. https://doi.org/10.18280/ts.380231
Joseph, J., Anoop, B. N., & Williams, J. (2019). A modified unsharp masking with adaptive threshold and objectively defined amount based on saturation constraints. *Multimedia Tools and Applications*, *78*, 11073-11089. https://doi.org/10.1007/s11042-018-6682-1
Kheradmand, A., & Milanfar, P. (2015). Non-linear structure-aware image sharpening with difference of smoothing operators. *Frontiers in ICT*, *2*, 22. https://doi.org/10.3389/fict.2015.00022
Kim, S., & Allebach, J. P. (2005). Optimal unsharp mask for image sharpening and noise removal. *Journal of Electronic Imaging*, *14*(2), 023005. https://doi.org/10.1117/1.1924510
Li, L., Wu, D., Wu, J., Li, H., Lin, W., & Kot, A. C. (2016). Image sharpness assessment by sparse representation. *IEEE Transactions on Multimedia*, *18*(6), 1085-1097. https://doi.org/10.1109/TMM.2016.2545398
Li, P., Wang, H., Yu, M., & Li, Y. (2021). Overview of image smoothing algorithms. *2nd International Conference on Computer Information and Big Data* (012024). Journal of Physics: Conference Series. https://doi.org/10.1088/1742-6596/1883/1/012024
Ngo, D., Lee, S., & Kang, B. (2020). Nonlinear unsharp masking algorithm. *2020 International Conference on Electronics, Information, and Communication (ICEIC)* (pp. 1-6). IEEE. https://doi.org/10.1109/ICEIC49074.2020.9051376
Osher, S., & Rudin, L. I. (1990). Feature-oriented image enhancement using shock filters. *SIAM Journal on Numerical Analysis*, *27*(4), 919-940. https://doi.org/10.1137/0727053
Jeevakala, S., & Therese, A. B. (2018). Sharpening enhancement technique for MR images to enhance the segmentation. *Biomedical Signal Processing and Control*, *41*, 21-30. https://doi.org/10.1016/j.bspc.2017.11.007
Sadah, Y. A., Al-Najdawi, N., & Tedmori, S. (2013). Exploiting hybrid methods for enhancing digital X-ray images. *International Arab Journal of Information Technology*, *10*(1), 28-35.
Sheppard, A. P., Sok, R. M., & Averdunk, H. (2004). Techniques for image enhancement and segmentation of tomographic images of porous materials. *Physica A: Statistical Mechanics and Its Applications*, *339*(1-2), 145-151. https://doi.org/10.1016/j.physa.2004.03.057
Shi, Z., Chen, Y., Gavves, E., Mettes, P., & Snoek, C. G. M. (2021). Unsharp mask guided filtering. *IEEE Transactions on Image Processing*, *30*, 7472-7485. https://doi.org/10.1109/TIP.2021.3106812
Simi, V. R., Edla, D. R., & Joseph, J. (2023). An inverse mathematical technique for improving the sharpness of magnetic resonance images. *Journal of Ambient Intelligence and Humanized Computing*, *14*, 2061-2075. https://doi.org/10.1007/s12652-021-03416-1
Singh, U., & Choubey, M. K. (2021). A review: image enhancement on MRI images. *2021 5th International Conference on Information Systems and Computer Networks (ISCON)* (pp. 1-6). IEEE. https://doi.org/10.1109/ISCON52037.2021.9702464
Venkatanath, N., Praneeth, D., Maruthi Chandrasekhar, Bh., Channappayya, S. S., & Medasani, S. S. (2015). Blind image quality evaluation using perception based features. *2015 Twenty First National Conference on Communications (NCC)* (pp. 1-6). IEEE. https://doi.org/10.1109/NCC.2015.7084843
Vin Toh, K. K., & Mat Isa, N. A. (2011). Locally adaptive bilateral clustering for image deblurring and sharpness enhancement. *IEEE Transactions on Consumer Electronics*, *57*(3), 1227-1235. https://doi.org/10.1109/TCE.2011.6018878
Vu, P. V., & Chandler, D. M. (2012). A fast wavelet-based algorithm for global and local image sharpness

estimation. *IEEE Signal Processing Letters*, *19*(7), 423-426. https://doi.org/10.1109/lsp.2012.2199980
Yang, C.-C. (2014). Finest image sharpening by use of the modified mask filter dealing with highest spatial frequencies. *Optik - International Journal for Light and Electron Optics*, *125*(8), 1942-1944. https://doi.org/10.1016/j.ijleo.2013.09.070
Zafeiridis, P., Papamarkos, N., Goumas, S., & Seimenis, I. (2016). A new sharpening technique for medical images using wavelets and image fusion. *Journal of Engineering Science and Technology Review*, *9*(3), 187-200. https://doi.org/10.25103/jestr.093.27
Zhang, R., & Wu, J. (2023). A bidirectional guided filter used for RGB-D maps. *IEEE Transactions on Instrumentation and Measurement*, *72*, 5009714. https://doi.org/10.1109/TIM.2023.3256467